One-dimensional nonlinear Schrödinger equation: A nonlinear dynamical approach

Yi Wan and C. M. Soukoulis
Ames Laboratory and Department of Physics, Iowa State University, Ames, Iowa 50011
(Received 26 May 1989)

We have studied a time-independent nonlinear Schrödinger equation of the tight-binding form on a one-dimensional lattice. The real and complex wave functions as solutions to the equation are considered separately for different physical problems. For each case, an area-preserving map for the discrete nonlinear Schrödinger equation is introduced and analyzed. The bounded solutions can be organized in hierarchies composed of periodic, quasiperiodic, as well as chaotic orbits on the phase plane of the nonlinear map. A "stability-zone" diagram, where the bounded orbits exist, is displayed in the parameter space, serving as "phase diagram" of the nonlinear Schrödinger equation under appropriate boundary conditions. Studies of the stability zone yield useful information for the physical problems considered. The periodic orbits and their stabilities can be obtained by a convergent perturbation method. Finally, we remark on several physical problems where these results might be applicable. In particular, we discuss the stabilities of the large polaron solution in the Holstein model.

I. INTRODUCTION

The nonlinear Schrödinger equation has been very useful in describing many physical systems involving nonlinearity, such as the propagation of classical waves in dispersive nonlinear media.[1] The common approach in dealing with these systems is to take advantage of the fact that in many cases the wave fields have small amplitudes and their envelopes vary slowly in space, so they can be approximately described by the continuum nonlinear Schrödinger equation and treated by perturbation methods. This strategy has also been used for physical systems with underlying crystalline structures, where the relevant order parameters are approximated by continuous mean-field variables.[1,2] However, in condensed-matter physics, the fundamental periodicity introduced by the discrete lattice is known to play an essential role, through the Bloch theorem, in our understanding of the properties of many important physical quantities. Although the effects of periodicity are not obvious in nonlinear systems due to lack of the principle of superposition, it is likely that they might have important consequences in certain cases. In this paper, we consider the problem of interplay of nonlinearity and periodicity by studying a particular type of the discrete nonlinear Schrödinger equation, i.e., a time-independent one-dimensional Schrödinger equation of the tight-binding form with a cubic nonlinear term,

$$-\psi_{n+1}-\psi_{n-1}-\lambda|\psi_n|^2\psi_n=E\psi_n \ , \tag{1}$$

where ψ_n is the complex "wave function" at the nth lattice site and E and λ are real parameters representing energy and nonlinear coupling constant, respectively. The underlying periodicity is expressed in the discrete form of Eq. (1). Equations of similar form have appeared in a number of physical models, including, among others, the lattice ϕ^4 theory of commensurate-incommensurate structural phase transitions,[2,3] Holstein's polaron model on molecular crystal chain,[4] electronic[5,6] and optical[7] responses on nonlinear lattice (superlattice), and, most recently, the mean-field theory of periodic array of twinning planes in the high T_c supeconducting oxides.[8] Under the continuum approximation, Eq. (1) is replaced by a second-order nonlinear differential equation, which is, in general, integrable via the inverse scattering transformation, and the solitary wave type of solutions often follow. However, in applying such a procedure, one often ignores completely the periodicity in the basic equation, along with its physical effects such as pinning of the order-parameter field by the lattice. On the other hand, the infinity of difference equations in Eq. (1) can be viewed as a nonlinear dynamical map where n denotes the discrete "time." More precisely, Eq. (1) belongs to the class of area-preserving nonlinear return maps on the Poincaré surface of section, describing nonlinear dynamics of two-degrees-of-freedom classical Hamiltonian systems. Much progress has been made in the studies of such nonlinear dynamical systems in the past two decades, and it is well known that they can exhibit rich and complex behavior, due to their nonintegrable characters. To see the difference between the continuum approximation and the nonlinear dynamical approach we rewrite Eq. (1) in the form of a "dynamical" equation,

$$-\frac{d^2\psi_t}{dt^2}=k^2\psi_t+\frac{\lambda k}{\sin k}|\psi_t|^2\psi_t\sum_n\delta(t-n) \ ,$$

$$E=-2\cos k$$

where ψ_t is now a function of the continuous variable t. In contrast to the continuum approximation, the presence of the t-dependent δ-function factor, expressing periodicity, makes the above equation nonintegrable. It

is our purpose, in this paper, to study the general properties of solutions to the discrete nonlinear Schrödinger equation by applying the concepts and methods developed for area-preserving nonlinear dynamical maps, in the hope that the results will be helpful in understanding particular physical models in which such an equation appears. We first study a simpler case, namely Eq. (1) in the real domain, where ψ_n is replaced by real variable x_n, satisfying

$$-x_{n+1}-x_{n-1}-\lambda x_n^3=Ex_n \ . \tag{2}$$

In Sec. II an area-preserving nonlinear map for Eq. (2) is analyzed in the context of nonlinear dynamical theory[9–15] and it is shown, based on the theories of Poincaré, Birkhoff, and the Kolmogorov-Arnold-Moser (KAM) theorem, that the bounded solutions to Eq. (2) correspond to periodic, quasiperiodic, and chaotic orbits on the phase plane of the map. It also proves useful to present, on the parameter plane (E,λ), the region where the bounded solutions exist. In Sec. III the periodic orbits are searched on the parameter space of Eq. (2), and a powerful "backward perturbation scheme" developed by Eminhizer, Helleman, and Montroll[16] that allows one to determine these orbits effectively is demonstrated. The complex case, Eq. (1), will be treated in Sec. IV, where it is first reduced to an area-preserving nonlinear map of a different form by utilizing its symmetry, then the resulting map is analyzed in a similar way. Finally, in Sec. V we summarize the results obtained in the previous sections and present some remarks on their physical significance.

II. NONLINEAR SCHRÖDINGER EQUATION IN REAL DOMAIN

The particular form of the area-preserving map for Eq. (2) can be written as

$$T:\ y'=x,\ \ x'=-y-x(\lambda x^2+E)\ , \tag{3}$$

such that for given λ and E, starting from the "initial point" (x_0,y_0) which is usually determined from the boundary conditions of a particular physical problem, a series of points $(x_n,y_n)=T^n(x_0,y_0)$ can be generated, forming an orbit on the phase plane (x,y). The same orbit is again subject to the rest of the boundary conditions and stability requirements imposed by the physical problem. An orbit which meets all these conditions is then taken as the physical solution to Eq. (2). Notice that not all orbits obtained by iterations of T are bounded, only the bounded orbits are considered to be the relevant solutions. We would also like to point out that there is a distinction in the meaning of stability for a particular orbit. As will be discussed next, the stability of an orbit of T means its linear stability measured by the value of its residue, whereas the corresponding solution's "physical stability" depends on whether such a solution minimizes a certain action of a physical system. In fact, it has been shown[17,18] that typically a linearly unstable orbit minimizes the action, while a linearly stable orbit corresponds to the saddle point. Thus, the physical relevance of an orbit must be examined in the particular problem, as will be discussed in Sec. V.

At this point, it is useful to summarize the general properties of map T. First of all we find that T is an analytic, area-preserving twist map. It is easy to check that its Jacobian $\det(DT)=1$, where DT is the linearization of T,

$$DT(x,y)=\begin{bmatrix} -(3\lambda x^2+E) & -1 \\ 1 & 0 \end{bmatrix} .$$

The eigenvalues of $DT(x,y)$ are determined by its trace. It follows that the stability of a periodic orbit is described by $\mathrm{Tr}(DT^q)=\mathrm{Tr}[\prod_{n=1}^{q}DT(x_n,y_n)]$, or equivalently by using Greene's residue[13,14] $R=\frac{1}{4}[2-\mathrm{Tr}(DT^q)]$. An orbit is stable (elliptic) when $0<R<1$, except for $R=\frac{3}{4}$ or $\frac{1}{2}$, while it is unstable when $R<0$ (hyperbolic) or $R>1$ (hyperbolic with reflection). According to Meiss,[15] the periodic orbits can be organized into classes. Geometrically, each point of an elliptic orbit on the phase plane is surrounded by nearby periodic orbits of higher classes, and also by the KAM invariant circles. The rate at which these nearby points rotate around the given elliptic orbit is also determined by its residue: $R=\sin^2(\omega\pi)$, where ω is the rotation frequency about one of its points. When the parameters of map T are varied, R and ω of the elliptic orbit will change, along with its position on the phase plane. Typically, whenever ω reaches a rational value, for instance p/q where p and q are co-prime-integers, bifurcations occur and new, higher class periodic orbits are born, which rotate around the fixed point of their parent orbit p times under iteration T^q. Typically at the bifurcation points, the elliptic orbit maintains its stability, and the nearby quasiperiodic orbits remain until its residue reaches unity $(\omega=\frac{1}{2})$ where the orbit loses its stablity by period-doubling bifurcation. However, there are exceptional cases occurring at the quadrupling and tripling bifurcation points $(R=\frac{3}{4}$ and $\frac{1}{2})$ where the elliptic orbits lose their stability temporarily. These details will be discussed later.

An important property of T is its reversibility and the related symmetries.[14,15] To show this, we write $T=T_1T_2$, where

$$T_1:\ x'=y,\ \ y'=x\ ,$$
$$T_2:\ x'=x,\ \ y'=-y-x(\lambda x^2+E)\ . \tag{4}$$

The involutions T_1 and T_2 satisfy $T_1^2=T_2^2=1$ so that T can be inverted: $T^{-1}=T_2T_1$. This implies the "time-reversal" symmetry of Eq. (2), since no explicitly n-dependent terms are present in the equation. One would expect violation of this symmetry when such terms exist, for instance, in the presence of a constant electric field. Sets of fixed points of T_1 and T_2, in general, form curves in the phase plane called symmetry lines. The symmetry line for T_1 is simply $x=y$, and for T_2 is $y=-\frac{1}{2}x(\lambda x^2+E)$. It follows that a periodic orbit of T is invariant under reflections by T_1 or T_2, since it is its own "time" reversal. The symmetry properties are very helpful in finding periodic orbits, since they require that the periodic orbit initially on the symmetry lines stay on

the line as the parameters are changed. Notice that reflections by T_1 or T_2 preserve the period and residue of the orbit. Also it is observed[14] that every time a point of a periodic orbit on a symmetry line undergoes a bifurcation, two point of the newborn orbit can be found on either the same line or the other. In our case, we found that the class-0 elliptic orbits which originate from the fixed point of T, $x=y=0$, tend to have points on the symmetry line of T_1, $x=y$, while the higher class periodic orbits in the period-doubling bifuraction series appear on that of T_2.

To study the oribts of T, first we consider $\lambda>0$ and use the scaled variables $(x,y)\rightarrow(x/\sqrt{\lambda},y/\sqrt{\lambda})$, so that λ no longer appears in T and an orbit is determined by choosing E and (x_0,y_0). In Fig. 1 we display the stability zone of map T on the parameter plane, which consists of the images of symmetry line $x=y$ under interactions of T. The stability zone represents all the bounded orbits generated by T starting from $x_0^2=y_0^2=\lambda$ on the symmetry line of T_1, or equivalently, the trajectories of Eq. (2) with zero "initial momenta." The importance of the stability zone is that it describes the stabilities of all the class-0 elliptic orbits, which are the continuations of the linear periodic solutions of Eq. (2) as λ is increased from zero, and thus serves as the "phase diagram" of the nonlinear Schrödinger equation. The numerical results we present here are only for positive λ, since for $\lambda<0$ the symmetry line for the class-0 elliptic orbits becomes $x=-y$. In fact, the stability zone in the latter case has the same shape as in Fig. 1 provided E is replaced by $-E$. In one of the physical problems we considered, namely the Holstein's molecular crystal model, such a relation between positive and negative λ represents the electron-hole conjugation.

In generating the stability zone, an upper limit is imposed in our numerical procedure so that only those orbits smaller than the upper limit are considered bounded. We found that the stability zone boundary is sensitive to neither the upper limit nor the number of iterations, as long as a moderate number of the order 10^2 is exceeded. In fact, the unbounded orbits diverge as $\exp(3^n)$ [when the cubic term in Eq. (2) is dominant]. On the phase plane, the bounded orbits are organized in a hierarchical structure of "islands around islands." Each elliptic orbit at the center of an island is surrounded by KAM invariant circles and satellites of higher class periodic orbits, forming the attraction basin of the elliptic orbit. The shape of the stability zone can be understood by studying the evolution of the periodic orbits as λ increases from zero. When $\lambda=0$, $(x,y)=(0,0)$ is the elliptic fixed point of T for $-2<E<2$ where $R=\sin^2(\omega_0\pi)=\frac{1}{2}+E/4$. In fact, the solutions to the linearized Eq. (2) in this case can be parameterized by a wave vector k in $[0,2\pi]$ so that the allowed energies, given by $E=-2\cos k$, form an "energy band" of the linear Schrödinger equation. When λ is increased from zero, each solution evolves from its corresponding linear form. Solutions with rational values of k become the elliptic orbits on the phase plane whose $\omega_0=k/2\pi$, while those with irrational k form the KAM invariant circles. As will be shown in Sec. III, when the parameters λ and E satisfy certain relations, the corresponding periodic solution can be expressed in terms of a single (fixed) frequency Fourier series whose Fourier amplitudes are gradually renormalized as λ is varied, giving rise to a curve in the stability zone. Several such curves for lower period orbits are shown in Fig. 1. It is evident that the attraction basins shrink as λ increases. Eventually these curves terminate at the zone boundary, when the corresponding periodic orbits reach the point $R=1$ and lose their stability, while the encircling invariant circles all disappear.

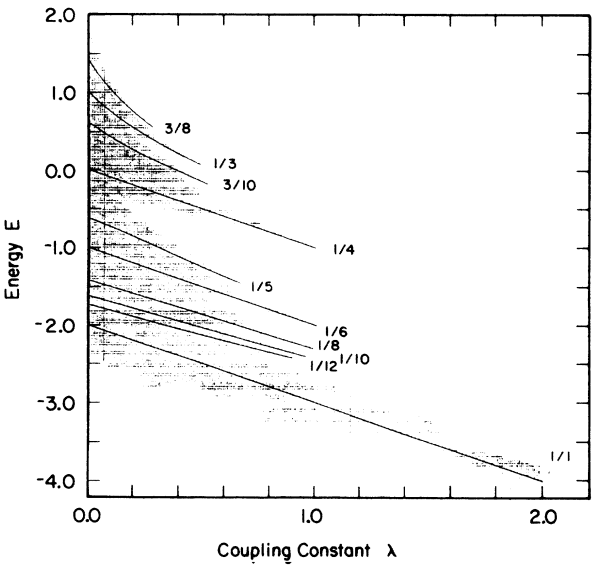

FIG. 1. "Stability zone" diagram on the parameter plane (E,λ), showing the regions for bounded (shaded) and divergent (unshaded) orbits of map T [Eq. (2)]. Solid curves represent elliptic orbits, each labeled with $\omega_0=p/q$.

Although the periodic orbits all together form only a zero-measure set among all orbits on the phase plane, they are dense everywhere on the plane and can trap other orbits around them. Thus, it appears that the structure of the stability zone can be understood in light of the periodic orbits and their stabilities. It should be noted that since the orbits of higher classes do not intersect the symmetry line $x=y$, the boundary of the stability zone in Fig. 1 is, in general, inside the true boundary of all bounded orbits. However, we expect it to be a good approximation to the latter because, as shown by Meiss,[15] the areas of the attraction basins of the higher class islands typically diminish at high rates as they approach their accumulation limits.

Before moving to the next section where periodic orbits will be our major concern, we discuss here the class-0 period-1 orbit which is simply the fixed point of T, but has the largest attraction basin (see Fig. 1). Two fixed points are born in a saddle-node bifurcation at $E=-2$ on the symmetry line of T_1,

$$x=y=\pm\sqrt{-2-E}\,,\quad R=-1-\frac{E}{2}\,. \tag{5}$$

On its route to the stability-zone boundary, the fixed point temporarily loses its stability in the quadrupling

and tripling bifurcations, at $E=-3.0$ and -3.5, respectively. The newborn orbits are not on the symmetry line $x=y$. As a result, there are cuts at the places of these bifurcations (see Fig. 1, similar features can be seen on other periodic orbits, e.g., on period-4 orbits in Fig. 2.). In the end, at $E=-4$, the fixed point loses its stability by period-doubling bifurcation. The dominant symmetry line for this period-doubling bifurcation series is found to be that of T_2. We have followed numerically the period-doubling bifurcation series up to the eighth bifurcation point as is shown in Table I. The period of the orbit between $(n-1)$th and nth bifurcation is 2^n, while the value of E at the nth bifurcation point is E_n, and Δx_n denotes the distance between the two points of the period-2^n orbit on the symmetry line at E_n, i.e., $x_{2^n}-x_{2^{n-1}}$. The numerical data in Table I indicate that E_n and Δx_n approach their accumulation points geometrically. From this behavior, two accumulation rates δ and α are obtained whose values indeed confirm the universality hypothesis for area-preserving dynamical maps.[3,14]

III. A PERTURBATION METHOD FOR PERIODIC ORBITS

To determine the periodic solutions of a nonlinear equation one usually performs perturbtive series analysis, as in a typical initial value problem. For Eq. (2) this amounts, for a given parameter E, to studying how amplitude and frequency of a periodic solution change when a small variation of (x_0,y_0) is made, i.e., moving horizontally on the stable zone diagram. However, for the nonintegrable nonlinear system the perturbation series, in general, diverges due to the presence of resonant denominators.[16] To overcome this difficulty, one has to modify the procedure of perturbation. Here we choose to start from the linear periodic solution and to find, for this particular orbit, its Fourier series as functions of both E and λ. In other words, we fix the central rotation frequency ω_0 of an orbit and look for its Fourier amplitudes renormalized as the parameters change in following the orbit. This procedure avoids the resonant denominators becasue the exact periodicity condition allows an expression of the orbit in terms of a single Fourier series. Such a "backward scheme" of perturbation was developed by Eminhizer *et al.*[16] and was successfully applied to the study of a system of coupled nonlinear oscillators. The results of our calculations for several of the lower-order class-0 periodic orbits are presented in Fig. 1 as curves traversing the stability zone, each labeled with $\omega_0=p/q$. In the following, we demonstrate the method for several cases.

A particular periodic orbit can be written in terms of a single frequency Fourier series,

$$x_n=\sum_{m=-\infty}^{\infty} A_m e^{im(2\pi n\omega_0+\delta)}, \tag{6}$$

where the Fourier amplitudes are real numbers satisfying $A_m=A_{-m}$, and δ is a phase to be fixed by the initial conditions $(x_0,y_0)=(x_0,x_{-1})$. Under Fourier transformation in Eq. (6), Eq. (2) becomes

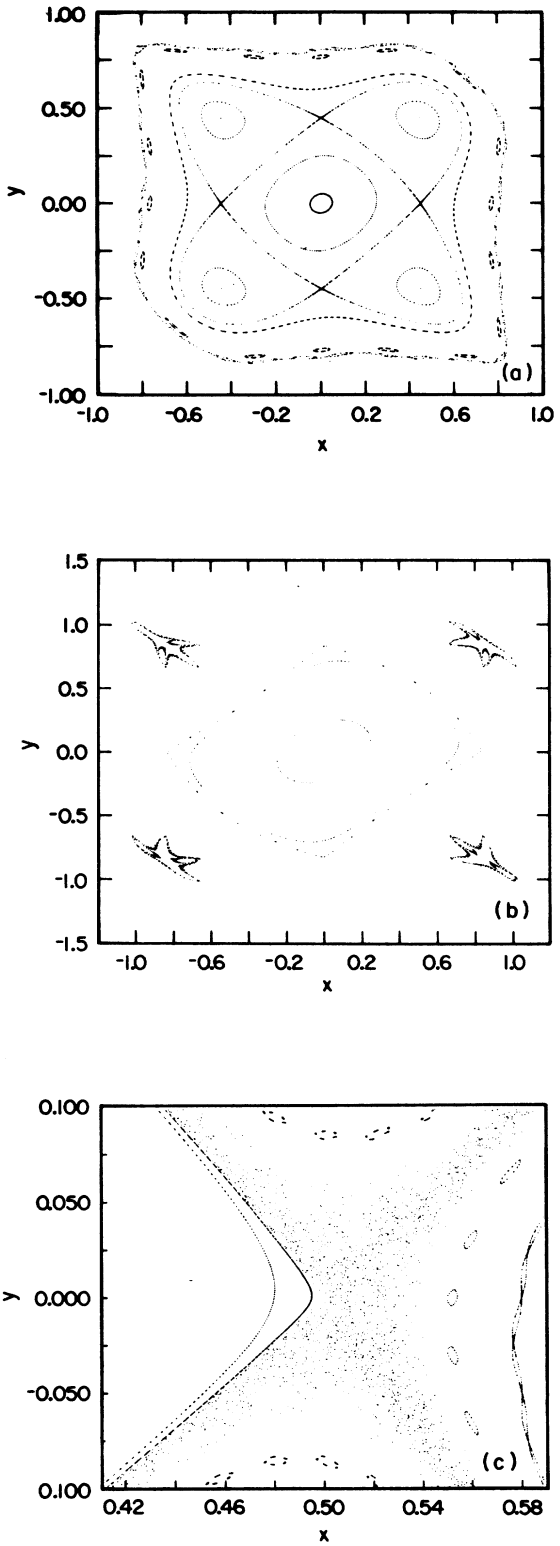

FIG. 2. (a) Period-4 elliptic and hyperbolic orbits and the surrounding invariant circles on the phase plane of map T at $E=-0.2$. Also shown are the separatrix connecting the hyperbolic period-4 orbit. (b) Period-4 elliptic orbit undergoing two pairs of period-doubling bifurcation at $E=-\sqrt{2}/2$. The newborn orbits are surrounded by invariant circles. (c) Chaotic orbit and invariant circles around the point (0.5,0.0) of the hyperbolic period-4 orbit at $E=-0.25$.

TABLE I. Period-doubling bifurcation series, where E_n denotes the value of E at the nth bifurcation point and Δx_n the distance between the points of the orbit at E_n. See discussions in the text.

Period (2^n)	E_n	Δx_n	$\delta_n=\frac{E_{n-2}-E_{n-1}}{E_{n-1}-E_n}$	$\alpha_n=\frac{\Delta x_{n-1}}{\Delta x_n}$
$2^0=1$	-4.0			
$2^1=2$	$-4.242\,640\,687\,119\,285\,1$	$-0.239\,146\,311\,738\,100\,3$		
$2^2=4$	$-4.270\,857\,563\,484\,179\,8$	$0.061\,647\,518\,939\,257\,2$	$8.599\,133\,510\,793\,571\,1$	$-3.879\,252\,820\,762\,129\,6$
$2^3=8$	$-4.274\,095\,612\,259\,405\,4$	$-0.015\,194\,932\,410\,526\,7$	$8.714\,160\,385\,965\,398\,4$	$-4.057\,110\,441\,409\,348\,8$
$2^4=16$	$-4.274\,466\,973\,111\,542\,2$	$0.003\,789\,773\,839\,156\,0$	$8.719\,413\,359\,254\,098\,9$	$-4.009\,456\,251\,328\,887\,0$
$2^5=32$	$-4.274\,509\,555\,467\,522\,9$	$-0.000\,942\,669\,911\,998\,5$	$8.721\,002\,950\,262\,201\,5$	$-4.020\,255\,437\,156\,702\,6$
$2^6=64$	$-4.274\,514\,438\,163\,561\,6$	$0.000\,234\,638\,167\,305\,8$	$8.721\,074\,513\,587\,251\,0$	$-4.017\,547\,199\,684\,414\,8$
$2^7=128$	$-4.274\,514\,998\,035\,401\,3$	$-0.000\,058\,393\,721\,734\,1$	$8.721\,095\,958\,882\,891\,5$	$-4.018\,208\,813\,170\,733\,0$
$2^8=256$	$-4.274\,515\,062\,232\,812\,1$	$0.000\,014\,532\,872\,680\,3$	$8.721\,096\,890\,406\,053\,6$	$-4.018\,043\,990\,246\,709\,2$

$$[2\cos(2\pi n\omega_0)+E]A_n=-\sum_{l,m}A_l A_m A_{n-1-m}\ . \tag{7}$$

For $\omega_0=p/q$ with p and q being co-prime-integers, we solve the above equations for the independent Fourier coefficients A_n with n in the range $-(q/2)<np<q/2$.

As an example, we first consider the period-4 orbit for which exact solutions can be obtained. The results are also shown in Fig. 2. Specifying $\omega_0=\frac{1}{4}$, we have A_0, A_1, and A_2 as the only independent Fourier amplitudes, and Eq. (7) reads

$$\begin{aligned}
-(2+E)A_0&=A_0^3+3(2A_0+A_2)A_1^2\\
&\quad+3A_2(A_0A_2+A_1^2)e^{i4\delta}\ ,\\
-EA_1&=3A_0^2A_1+6A_0A_1A_2+3A_1A_2^2e^{i4\delta}\\
&\quad+A_1^3(3+e^{-i4\delta})\ ,\\
(2-E)A_2&=3(A_0+2A_2)A_1^2+3A_0^2A_2\\
&\quad+3A_0A_1^2e^{-i4\delta}+A_2^3e^{i4\delta}\ .
\end{aligned}\tag{8}$$

The condition for the reality of $\{A_n\}$ and the initial condition $x_0=x_{-1}=\sqrt{\lambda}$ uniquely determine the quantities we are looking for, $A_0=A_2=0$, $A_1=\sqrt{-(E/2)}$, and $\delta=-(\pi/4)$, so that

$$x_n=\sqrt{-2E}\cos\left[\frac{\pi}{2}n-\frac{\pi}{4}\right],\quad R=4E^2(1-E^2)\ . \tag{9}$$

This is simply a straight line $\lambda=-E$ on the stability-zone diagram. If one requires that all the coefficients be nonzero and solves Eq. (8), one will find a lengthy expression for an orbit on the symmetry line of T_2, describing the period-4 orbit born after the second period-doubling bifurcations. Thus as λ increases from zero, the elliptic period-4 orbit starts at $E=0$ where $R=0$, passing the marginal point $R=1$ at $E=-(1/\sqrt{2})$, and continues until R decreases to zero at the stability-zone boundary where $E=-1$. After this, it becomes hyperbolic with negative residue. Such a journey of R is typical for all the even-period elliptic orbits, in constrast to the odd-period ones for which R eventually exceeds 1 and the corresponding oribts are hyperbolic with reflection. To explain this, consider a period-q_1 elliptic orbit with even q_1, each point (x_n,y_n) of the orbit is a fixed point of T^{q_1}. If, however, this orbit contains another elliptic orbit half of its period such that $T^{q_1}(x_n,y_n)=T^{2q_2}(x_n,y_n)$, then their residues are related by $R_{q_1}=4R_{q_2}(1-R_{q_2})$ and R_{q_1} will pass 1 and return to zero while R_{q_2} rises monotonically from zero to 1. The above period-4 orbit indeed presents such a case where $R_2=1-E^2$, $R_1=\frac{1}{2}(1-E)$, and R_4 is given in Eq. (9). This behavior results in the cuts on the branch of period-4 orbits in Fig. 1, occurring at $E=-1/\sqrt{2}$ with $R_4=1$, and $E=-\sqrt{3}/2$ with $R_4=3/4$, where there are pairs of period-doubling [see Fig. 2(b)] and period-tripling bifurcations, respectively.

The period-4 hyperbolic orbit can also be easily determined by choosing $\delta=\pi/2$

$$x_n=\sqrt{-E}\cos\left[n\frac{\pi}{2}+\frac{\pi}{2}\right],\quad R=-E^2(2+E^2)\ . \tag{10}$$

The chaotic orbits around it are shown in Fig. 2(c), which are surrounded by the invariant KAM circles and do not escape to infinity.

It is clear that for orbits of higher periods more Fourier components are involved, thus more equations need to be solved. In general, only serial solutions are available for most of the periodic orbits. We now outline this perturbative approach. Since the period-q orbit originates in the neighborhood of elliptic fixed point (0,0), where its amplitudes are small and where E is close to $-2\cos(2\pi\omega_0)$ we use a relocated form of Eq. (7) and introduce a parameter ϵ to indicate the orders of the serial solution,

$$\begin{aligned}
&x_{n+1}+x_{n-1}-2\cos(2\pi\omega_0)x_n\\
&\qquad=\epsilon\{-[2\cos(2\pi\omega_0)+E]x_n-x_n^3\}\ .
\end{aligned}\tag{11}$$

We attempt a solution of the form

$$x_n=\sum_{j=1}^{\infty}\epsilon^j\sum_{m=-\infty}^{\infty}A_m e^{im(2\pi n\omega_0+\delta)}\ , \tag{12}$$

with the conditions $A_m^{(j)}=A_{-m}^{(j)}$ and $A_m^{(j)}=0$ if $|m|>2j+1$, which leads to the following equation:

$$2[\cos(2\pi n\omega_0)-\cos(2\pi\omega_0)]A_n^{(j)} = -[2\cos(2\pi\omega_0)+E]A_n^{(j-1)} - \sum_{\{n,j-1\}} A_{n_1}^{j_3}A_{n_2}^{j_3}A_{n_3}^{j_3} , \tag{13}$$

where the summation runs over n_1,n_2,n_3 and j_1,j_2,j_3 under the constraints $n_1+n_2+n_3=n$ and $j_1+j_2+j_3=j-1$. The zeroth-order solutions for $j=0$, $n=0,\pm1$ are $A_0^{(0)}=0$ and $A_{\pm1}^{(0)}\neq0$, to be determined by higher-order equations.

In solving these higher-order equations, we take as example one of the even-period orbits. Specifying $\omega_0=p/q$, it follows that $A_{2n}=0$ for even q, while for odd-period orbits, such as those with $\omega_0=1/3,1/5$, A_{2n}, especially A_0 will resume nonzero values from the higher-order contributions. The reason for this is that only one point of an odd-period orbit appears on the symmetry line of T_1, whereas there are two such points for an even-period orbit. Thus, unlike an even-period orbit, the class-0 odd-period orbits are not symmetric under reflection about the line $y=-x$, which is perpendicular to the symmetry line $x=y$. The nonzero coefficients are given as follows: For $j=1$, $n=0,\pm1,\pm2,\pm3$,

$$A_1^{(0)2}=-\tfrac{1}{3}(E+2\cos\omega_0) ,$$

$$A_3^{(1)}=-\frac{A_1^{(0)3}}{2[\cos(3\omega_0)-\cos\omega_0]} ;$$

for $j=2$, $n=0,\pm1,\pm2,\pm3,\pm4,\pm5$,

$$A_1^{(1)}=-\tfrac{1}{2}A_3^{(1)} ,$$

$$A_3^{(2)}=\tfrac{3}{2}\frac{A_3^{(1)2}}{A_1^{(0)}} ,$$

$$A_5^{(2)}=-3A_3^{(1)}A_1^{(0)2} .$$

To complete the second-order solutions we derive from the $j=3$ equations $A_1^{(2)}=-\frac{13}{8}A_3^{(2)}$. It is evident from $A_1^{(0)}$ that E decreases from its value for the corresponding linear solution, $-2\cos(2\pi\omega_0)$ as nonlinearity increases. Also, the above expressions for $A_n^{(j)}$ indicate that the Fourier series converges rapidly for the parameter values inside the stability zone. We use these Fourier components to construct the periodic solutions with various even periods and found that the results are already accurate enough for our purposes.

IV. NONLINEAR SCHRÖDINGER EQUATION IN COMPLEX DOMAIN

Writing $\psi_n=x_n+iy_n$, Eq. (1) becomes

$$\begin{aligned} -x_{n+1}-x_{n-1}-\lambda(x_n^2+y_n^2)x_n&=Ex_n ,\\ -y_{n+1}-y_{n-1}-\lambda(x_n^2+y_n^2)y_n&=Ey_n . \end{aligned} \tag{14}$$

In contrast to the real wave-function case [Eq. (2)], Eq. (14) contains two coupled second-order difference equations for the real variables, and represents a nonlinear map in the four-dimensional phase space $(x_{n-1},x_n,y_{n-1},y_n)$. A problem that might arise for such a nonlinear map involves the so-called Arnold's diffusion which is known to exist, in general, in nonlinear dynamical systems with degrees of freedom greater than 2. As a consequence, one cannot guarantee the existence of a particular bounded orbit (x_n,y_n) over aribtrary distance on the lattice. However, as we will show next, because of the conservation of probability current implied in Eq. (1), this four-dimensional map can be reduced to two dimensional, and the possibility of Arnold's diffusion is thus ruled out.

In order to derive the reduced map, we write the wave function and Eq. (1) in polar coordinates $\psi_n=r_ne^{i\theta_n}$ and

$$\begin{aligned} r_{n+1}\cos(\Delta\theta_{n+1})+r_{n-1}\cos(\Delta\theta_n)&=2f(r_n) ,\\ r_{n+1}\sin(\Delta\theta_{n+1})-r_{n-1}\sin(\Delta\theta_n)&=0 , \end{aligned} \tag{15}$$

where $\Delta\theta_n=\theta_n-\theta_{n-1}$ and $f(r)=-\frac{1}{2}r(\lambda r^2+E)$. The second equation defines an integral of motion for Eq. (15)

$$J\equiv r_nr_{n-1}\sin(\Delta\theta_n) , \tag{16}$$

which has the physcial meaning of probability current. Following Bountis and co-workers[19] in their study of a model for colliding proton beams in the storage ring, we introduce new variables,

$$\begin{bmatrix} u_n\\ v_n \end{bmatrix}=\begin{bmatrix} r_n^2\\ J\cot(\Delta\theta_n) \end{bmatrix} . \tag{17}$$

The reduced map S follows from Eq. (16) and the first equation in Eq. (15)

$$S:\ u_{n+1}=\frac{1}{u_n}(v_{n+1}^2+J^2),\quad v_{n+1}=-v_n-u_n(u_n+E) , \tag{18}$$

where its variables have been scaled by the nonlinear coupling constant λ: $(u,v)\to(\lambda u,\lambda v)$, and λ is absorbed into J: $J\to\lambda J$. Besides E, J is the only other parameter in S, which describes the strength of the nonlinearity and is to be determined from λ and the "initial conditions." Map S is related to Eq. (1) as follows. Once ψ_0 and ψ_1 are known in a particular physical problem, r_0, r_1, θ_0, and θ_1, are found immediately. Then J follows from Eq. (16), and (u_1,v_1) is used to initiate the iterations in Eq. (18). Reversely, r_n and $\Delta\theta_n$ (in $[0,\pi]$ or $[\pi,2\pi]$, respectively, for positive or negative J) can be obtained directly from (u_n,v_n), and $\theta_n=\sum_{m=0}^{n}\Delta\theta_m$, for any n. This procedure enables us to study the solutions of Eq. (1) in terms of the (bounded) orbits of map S on the phase plane (u,v). For the special case $J=0$, we use directly Eq. (14) which is now decoupled and returns to the case of Secs. II and III.

Map S shares the properties we discussed for map T. Indeed, S is area preserving for every periodic orbit, since $\det(DS^q)=\prod_{n=1}^{(q)}\det[DS(u_n,v_n)]=1$, where $\det[DS(u_n,v_n)]=(u_{n+1})/(u_n)$. The reversibility is similarly expressed as $S=S_2S_1$, where

$$\begin{aligned} S_1:&\ u'=\frac{1}{u}(v^2+J^2),\quad v'=v ,\\ S_2:&\ u'=u,\quad v'=-v-u(u+E) . \end{aligned} \tag{19}$$

The involutions satisfy $S_1^2=S_2^2=1$ so that $S^{-1}=S_1S_2$. Geometrically on the phase plane, S_1 has the effect of "inversion" along the u axis about the $u>0$ branch of hyperbola $u^2-v^2=J^2$, and S_2 represents a reflection about the parabola $v=-\frac{1}{2}u(u+E)$ along the v axis (cf. Fig. 4). The two curves $u=(v^2+J^2)^{1/2}$ and $v=-\frac{1}{2}u(u+E)$ are the symmetry lines of S_1 and S_2, respectively.

The analysis of map S follow closely what we did in Sec. II. We construct the stability zone for map S. We choose the initial point $r_0=r_1=\sqrt{\lambda}$, $\theta_0=0$, $\theta_1=k$, corresponding to (u_0,v_0) on the symmetry line of S_1. However, we have now three independent parameters to be specified, namely, E, λ, and k. In order to present the stability zone on the parameter plane (E,λ) we select k in the following way. $E=-2\cos k$ when $-2\le E\le 2$, and $k=2\pi/100$ when $E<-2$. Such a choice of k does not affect our purpose of understanding the structures of the solutions. Besides, it presents a typical situation in the nonlinear transmission problem we have studied. In addition, we consider only positive values for λ for which we found no bounded solutions when $E>2$. For negative λ, one discovers the same stability zone provided k is replaced by $\pi+k$. It is interesting to see that the stability zone in this case (Fig. 3) resembles the shape found in Fig. 1. Also shown are curves for some of the lower-order class-0 period elliptic orbits. In Fig. 4, we plot the elliptic and hyperbolic period-5 orbits, and the surrounding invariant circles and chaotic orbits. Notice how the orbits are arranged about the two symmetry lines. In fact the symmetry lines make it much easier to locate numerically a periodic orbit. Since the starting point of the iterations (u_0,v_0) is always on the symmetry line of $S_1, u_1=(v_1^2+J^2)^{1/2}$, it is sufficient to do a one-dimensional search for a particular periodic orbit.

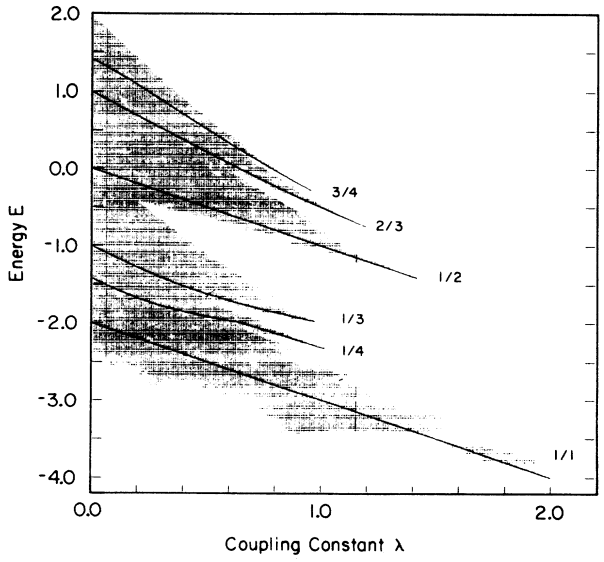

FIG. 3. "Stability zone" diagram on the parameter plane (E,λ) for map S [Eq. (1)], similar to Fig. 1. Solid curves represent elliptic orbits, each labeled with $\omega_0=p/q$.

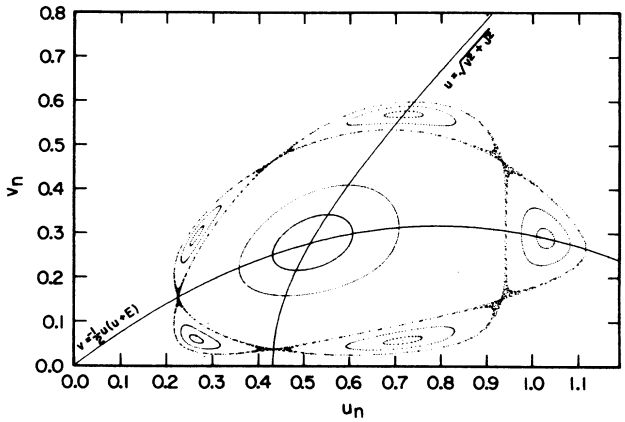

FIG. 4. Period-5 elliptic and hyperbolic orbits at $E=-1.598$, with their surrounding chaotic orbits and invariant circles on the phase plane (u,v) of map S. The solid curves are the symmetry lines of S_1 and S_2.

V. CONCLUSIONS AND DISCUSSIONS

In the preceding sections we have shown that the one-dimensional discrete nonlinear Schrödinger equation can be treated as area-preserving nonlinear dynamical maps in both real and complex domains. As a result, its solutions share the universal properties of the typical two-degrees-of-freedom Hamiltonian system. The typical behavior of the solutions can be summarized in terms of the stability-zone diagrams over the entire ranges of the parameters. Although such diagrams are constructed for a particular type of boundary conditions, namely the solutions they present must intersect the symmetry lines, it is clear that the primary features will emerge in many other problems involving the nonlinear Schrödinger equation. These features revealed in our study are in contrast to the traditional continuum approximation approaches used in solving this type of equation where, for instance, the analyticity of the solutions eliminates the possibility of chaotic states and the fractal structures of the stability zones. Moreover, our results might provide some guidance to the applicability of the continuum approximation, since the magnitudes of the parameters in the problem, such as the nonlinear coupling constant or the amplitudes of the solutions are not the only factors to be considered in applying the continuum approximation. It is clear to Figs. 1 and 3 that the linear periodic solutions can survive even in the region of strong nonlinearity. In fact, in the attraction basins of these elliptic orbits, the nearby KAM invariant circles are well behaved as shown in Fig. 5 in the real space of the lattice, recovering the soliton arrays obtained in the continuum approximation. For small nonlinearity, these attraction basins, especially from the lower-period orbits, would dominate the stability zone, so it seems reasonable to expect such smooth solutions to prevail in the corresponding physical problems. Indeed, when E is in the "energy band" of the linearized Eq. (1), $-2<E<2$, the smooth solutions can be obtained under the continuum approximation by treating nonlinear terms as small perturbations. However, when $E<-2$, one enters the genuinely nonperturbative

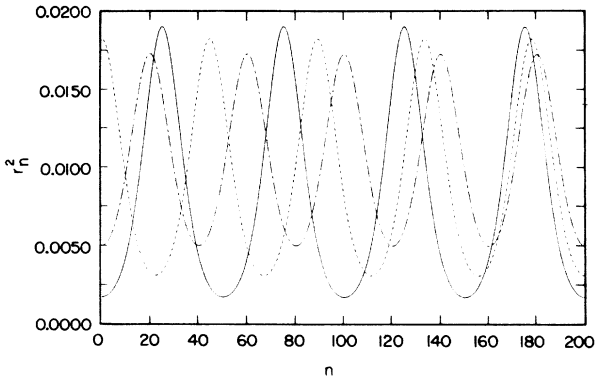

FIG. 5. r_n^2 as function of the lattice site n on a segment of the lattice. $E=-2.01$, $k=2\pi/100$, and $\lambda=1.7\times10^{-3}$(——), 3.1×10^{-3}(— — —), and 5.0×10^{-3}(— · — · —), respectively, for the three states, corresponding to the weak nonlinearity regime where continuum approximation is valid.

regime where the linear solutions are themselves unstable and it is necessary to make the continuum approximation or perturbation expansions about the elliptic orbits. This information is provided in our studies of the stability zone and the periodic solutions using the backward perturbation technique. When nonlinearity increases, approaching the boundary of the stability zone, the attraction basins of the elliptic orbits shrink while the chaotic regions surrounding the hyperbolic orbits grow and become connected as the invariant circles disappear. Finally, one moves into the region of escaping orbits. A typical chaotic solution is shown in Fig. 6, in contrast to the smooth solutions of Fig. 5, no analytic envelope function can be found for such a solution. A transition from effectively weak to strong nonlinearity has also been studied in other nonlinear systems. For instance, in the well-known Fermi-Pasta-Ulam model where it is shown[20] that as the energy density (or equivalently, the initial amplitudes) is raised, the soliton solutions obtained from the continuum [Korleweg–de Vries (KdV)] equation are eventually replaced by the chaotic, energy-equipartition modes.

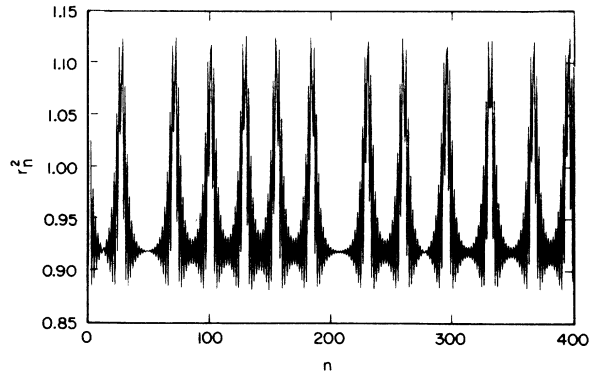

FIG. 6. Similar to Fig. 5, but for $E=-1.0$, $k=\pi/3$, and $\lambda=1.0593$, chaotic orbit around the period-2 hyperbolic orbit.

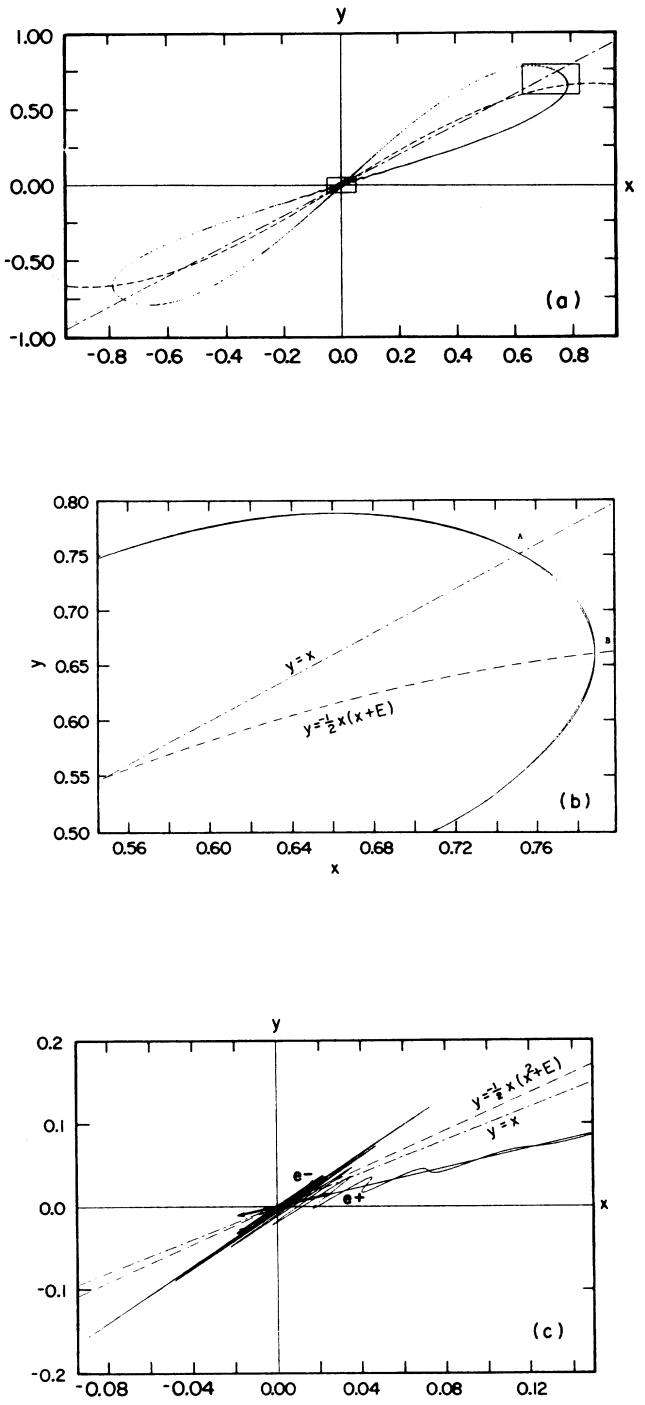

FIG. 7. (a) Separatrix of the fixed point of map T at $E=-2.25$, where dashed and dot-dashed curves denote the symmetry lines. (b) Enlargement of the larger rectangle shown in (a), showing the splitting separatrices and several homoclinic points. Also shown are the symmetry lines intersecting the separatrices at the two homoclinic points labeled A and B. (c) Enlargement of the smaller rectangle shown in (a), showing the stable separatrix wandering about the unstable one, only a segment of the separatrices is drawn to keep the figure legible. Arrows denote the eigenvectors of the hyperbolic fixed point.

Applying the results obtained in the preceding sections, we have studied elsewhere[6] the problem of wave transmissions in a finite one-dimensional nonlinear lattice described by Eq. (1). The information gathered from the stability zone and the structures of the periodic orbits proves to be essential in explaining the numerically observed features in the transmission coefficient, such as bistable and noisy responses. Here, as an example, we consider briefly a different physical problem, namely, Holstein's large polaron model,[4] which provides a case for our discussions of the physical stability[17,18] of the solutions and the effects of periodicity of the lattice. Holstein's large polaron is described by the solution to Eq. (1) which minimizes the following energy functional of the system:

$$E_T[\{\psi_m\}]=-\sum_n [\tfrac{1}{2}\lambda|\psi_n|^4+\psi_n^*(\psi_{n-1}+\psi_{n+1})] , \quad (20)$$

where $\lambda=A^2/t_0 M\nu^2$, where A is the adiabatic electron-phonon coupling constant, M and ν are, respectively, mass and frequency of the diatomic molecules which form the underlying lattice chain, and t_0 denotes the electronic hopping matrix element which is also the unit of E_T. The normalization condition of the electron wave function on infinite lattice $\sum_n|\psi_n|^2=1$ requires the large polaron solution to vanish for $n\to\pm\infty$. It can be easily shown that, for such a solution, Eq. (1) reduces to Eq. (2), which is readily solved under the continuum approximation by the following self-trapped minimal energy solution:

$$x_n=\pm\sqrt{(\lambda/8)}\,\mathrm{sech}[(n-\xi)/l_p] , \quad (21)$$

where n is now a continuous variable. The electronic energy of the large polaron is given by $E=-2-(\lambda/4)^2$, and $l_p=4/\lambda$ is the polaron's width. The free parameter ξ specifies the polaron's centroid position, implying the translational invariance of such a solution.

On the other hand, the large polaron as the solution of the discrete Eq. (2) is shown in Fig. 7 on the phase plane the map T. More precisely, it is described by the separatrix around the hyperbolic fixed point $x=y=0$ of T. For small λ, the separatrix looks like a single smooth curve, and is indeed very well approximated by Eq. (21). However, it is known that non-integrable nonlinear maps allow no such curve. Instead, the curve splits into two stable and unstable separatrices intersecting each other at the so-called homoclinic points [Fig. 7(b)]. The stable and unstable separatrices map onto each other by the involutions T_1 and T_2. As a result, there must be a homoclinic point on each of the two symmetry lines. Starting from these two points, one can generate an infinite set of homoclinic points by iterations of T and T^{-1}, which correspond to the only possible bound state of Eq. (2). Consequently, the large polaron state is represented asymptotically by the set of homoclinic points and is defined only on the discrete lattice sites, implying a reduced translational symmetry corresponding to translations in the unit of the lattice constant. Furthermore, since the distances between two homoclinic points diminish to zero when the hyperbolic fixed point is approached [cf. Fig. 7(c)], the lengths of the separatrix loops connecting the two points diverge to preserve the area they encircle, and any small perturbation would set off the asymptotic solution into wandering along with the separatrices. Indeed, for large enough λ, the separatrices become chaotic orbits confined by the nearby invariant circles in a narrow region on the phase plane. Physically, this means that even though Eq. (21) presents a reasonable continuum approximation to the large polaron state for small λ (when the chaotic region is very thin), it is unstable against the pinning of the discrete lattice and will eventually break into an array of randomly pinned small polarons. Thus, we conclude that the self-trapped solution alone, Eq. (21), cannot serve as the lowest-order approximation to the Holstein model, when the lattice periodicity is taken into consideration. Nonadiabatic effects must be carefully included before one proceeds to consider higher-order corrections.[21] We also point out that a transition from large to small polaron would occur before the continuum approximate solution in Eq. (21) breaks down, when λ is so large that the polaron's width becomes comparable to the lattice constant, $l_p\approx 1$.

ACKNOWLEDGMENTS

The authors acknowledge useful discussions with E. N. Economou, Gary Grest, and N. Papanicolaou. Ames Laboratory is operated for the U.S. Department of Energy by Iowa State University under Contract No. W-7405-Eng-82. This work was supported by the Office of Basic Energy Sciences, U.S. DOE. This work was partially supported by a North Atlantic Treaty Organization Grant No. RG674188.

[1]R. K. Dodd, J. C. Eilbeck, J. D. Gibbon, and H. C. Morris, *Soliton and Nonlinear Wave Equations* (Academic, London, 1984).
[2]Per Bak, Rep. Prog. Phys. **45**, 587 (1982).
[3]Per Bak and M. H. Jensen, J. Phys. A **15**, 1893 (1982).
[4]T. D. Holstein, Ann. Phys. (N.Y.) **8**, 325; **8**, 343 (1959).
[5]F. Delyon, Y. E. Levy, and B. Souillard, Phys. Rev. Lett. **57**, 2010 (1986).
[6]Yi Wan and C. M. Soukoulis, Phys. Rev. B **40**, 12264 (1989).
[7]Wei Chen and D. L. Mills, Phys. Rev. Lett. **58**, 160 (1987).
[8]A. A. Abrikosov, A. I. Buzdin, and M. L. Kulić, Supercond. Sci. Technol. **1**, 260 (1989).
[9]V. I. Arnold and A. Avez, *Ergodic Problems of Classical Mechanics* (Benjamin, New York, 1968).
[10]A. J. Lichtenberg and M. A. Lieberman, *Regular and Stochastic Motion* (Springer-Verlag, New York, 1983).
[11]B. V. Chirikov, Phys. Rep. **52**, 263 (1979).
[12]R. H. G. Helleman, in *Universality in Chaos,* edited by P. Critanović (Hilger, Bristol, 1984).
[13]J. M. Greene, J. Math. Phys. **20**, 6; **20**, 1183 (1979).
[14]J. M. Greene, R. S. MacKay, F. Vivaldi, and M. J. Feigenbaum, Physica D **3**, 468 (1981).
[15]James D. Meiss, Phys. Rev. A **34**, 2375 (1986).
[16]Charles R. Eminhizer, Robert H. G. Helleman, and Elliot W. Montroll, J. Math. Phys. **17**, 121 (1976).
[17]S. Aubry, Physica D **7**, 240 (1983); S. Aubry and P. Y. Le

Daeron, *ibid.* **8**, 381 (1983).
[18]R. S. Mackay and J. D. Meiss, Phys. Lett. A **98**, 92 (1983).
[19]T. C. Bountis, C. R. Eminhizer, and R. H. G. Helleman, in *Long-Time Prediction in Dynamics,* edited by C. W. Horton, Jr., L. E. Reichl, and V. G. Szebehely (Wiley, New York, 1983).
[20]S. Isola, R. Livi, S. Ruffo, and A. Vulpiani, Phys. Rev. A **33**, 1163 (1986).
[21]L. A. Turkevich and T. D. Holstein, Phys. Rev. B **35**, 7474 (1987); T. D. Holstein and L. A. Turkevich, *ibid.* **38**, 1901 (1988).

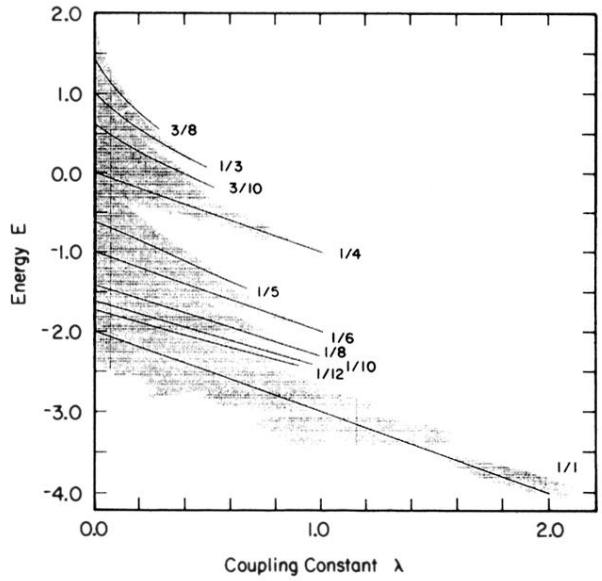

FIG. 1. "Stability zone" diagram on the parameter plane (E,λ), showing the regions for bounded (shaded) and divergent (unshaded) orbits of map T [Eq. (2)]. Solid curves represent elliptic orbits, each labeled with $\omega_0 = p/q$.

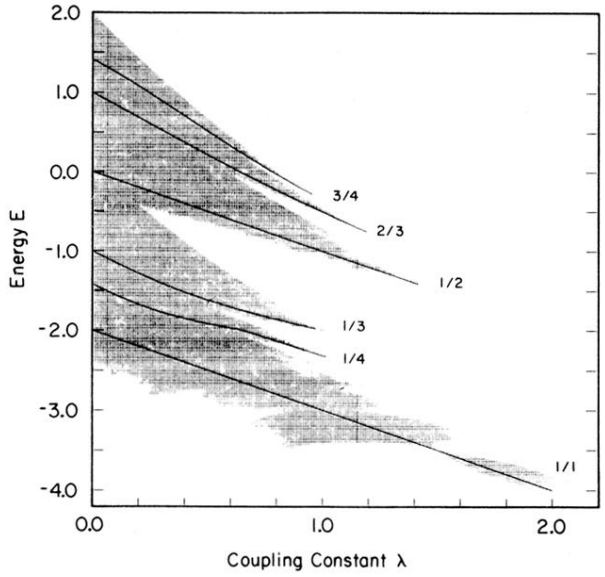

FIG. 3. "Stability zone" diagram on the parameter plane (E,λ) for map S [Eq. (1)], similar to Fig. 1. Solid curves represent elliptic orbits, each labeled with $\omega_0 = p/q$.